Chapter 2
Basic Ingredients for Modeling Chemical Evolution

2.1 Basic Ingredients

The basic ingredients for modeling galactic chemical evolution can be summarized as follows:

- Initial conditions
- The stellar birthrate function
- The stellar yields (nucleosynthesis)
- Gas flows (infall, outflow)

When all these ingredients are provided, we need to write a set of equations describing the evolution of the gas and its chemical abundances which include all of them. These equations will describe the temporal and spatial variation of the gas content and its abundances by mass (see next chapters).

The chemical abundance by mass of a generic chemical species i, is defined as:

$$X_i = \frac{M_i}{M_{\rm gas}}. \tag{2.1}$$

According to this definition, it holds:

$$\sum_{i=1,n} X_i = 1, \tag{2.2}$$

where n represents the total number of chemical species. Generally, in theoretical studies of stellar evolution, it is common to adopt X, Y, and Z as indicative of the abundances by mass of hydrogen (H), helium (He), and metals (Z), respectively. The baryonic Universe is made mainly by H and some He, while only a very small fraction resides in metals (all the elements heavier than He). However, the history of the growth of this small fraction of metals is crucial for understanding how stars and galaxies were formed and subsequently evolved.

F. Matteucci, *Chemical Evolution of Galaxies*, Astronomy and Astrophysics Library,
DOI 10.1007/978-3-642-22491-1_2, © Springer-Verlag Berlin Heidelberg 2012

2.1.1 Initial Conditions

The initial conditions for a model of galactic chemical evolution consist in establishing whether: (a) the chemical composition of the initial gas is primordial or pre-enriched by a pre-galactic stellar generation; (b) the studied system is a closed box or an open system (infall and/or outflow).

2.1.2 The Birthrate Function

The number of stars formed in the mass interval $m, m + \mathrm{d}m$ and in the time interval $t, t + \mathrm{d}t$ is the so-called *birthrate function* $B(m, t)$.

The birthrate function can be expressed as:

$$B(m, t) = \psi(t)\varphi(m), \tag{2.3}$$

where the quantity:

$$\psi(t) = \mathrm{SFR} \tag{2.4}$$

is called the star formation rate (SFR), namely, the rate at which the interstellar gas is turned into stars per unit time, and the quantity:

$$\varphi(m) = \mathrm{IMF} \tag{2.5}$$

is the initial mass function (IMF), namely, the mass distribution of the stars at birth.

2.1.2.1 The Star Formation Rate

The SFR indicates how many solar masses of gas transform into stars per unit time, and it is generally expressed in terms of $M_\odot\ \mathrm{yr}^{-1}$, $M_\odot\ \mathrm{pc}^{-2}\ \mathrm{yr}^{-1}$ or $M_\odot\ \mathrm{kpc}^{-2}\ \mathrm{yr}^{-1}$.

The most common parametrization of the SFR is the Schimdt–Kennicutt law:

$$\psi(t) = \nu\sigma_{\mathrm{gas}}^{k}, \tag{2.6}$$

where σ_{gas} is the gas surface density and $k = 1 - 2$ with a preference for $k = 1.4 \pm 0.15$ for spiral disks (see Fig. 2.1), and ν is a parameter describing the star formation efficiency, in other words, the SFR per unit mass of gas, and it has the dimensions of the inverse of a time. Other important physical quantities such as gas temperature, viscosity, and magnetic field are usually ignored.

Other common parametrizations of the SFR include a dependence on the total surface mass density (σ_{tot}) besides the surface gas density:

$$\psi(t) = \nu\sigma_{\mathrm{tot}}^{k_1}\sigma_{\mathrm{gas}}^{k_2}, \tag{2.7}$$

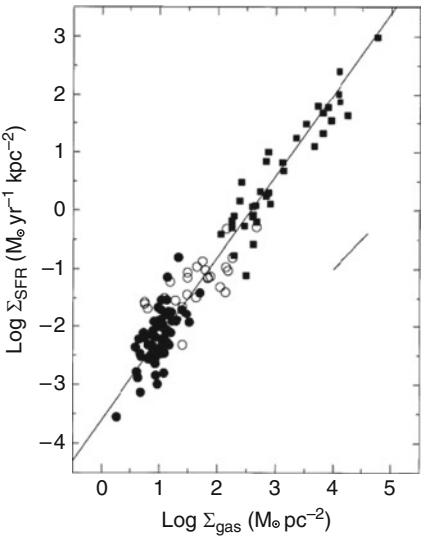

Fig. 2.1 The SFR as measured by Kennicutt (1998a) in star forming galaxies. The *continuous line* represents the best fit to the data and it can be achieved either with the SF law in (2.6) with $k = 1.4$ or with the star formation law in (2.10). The short, *diagonal line* shows the effect of changing the scaling radius by a factor of 2. Figure from Kennicutt (1998a); reproduced by kind permission of R.C. Jr. Kennicutt

with $k_1 = 1/3$ and $k_2 = 5/3$, as suggested by observational results of Dopita and Ryder (1994) and taking into account the influence of the potential well in the star formation process (i.e., feedback between SN energy input and star formation) as suggested first by Talbot and Arnett (1975):

$$\psi(t) = \nu_\odot [\sigma_{\rm tot}\sigma_{\rm gas}/\sigma_\odot^2]^{k-1}\sigma_{\rm gas}, \tag{2.8}$$

where $\nu = \nu_\odot [\sigma_{\rm tot}\sigma_{\rm gas}/\sigma_\odot^2]^{k-1}$ is the efficiency of star formation, and $\nu_\odot$ and $\sigma_\odot$ are the star formation efficiency and the total surface mass density at the solar ring, respectively. These latter quantities were originally introduced as normalization constants but in reality they play the role of a radial scale controlling the star formation process. This formulation was based on the original Schmidt (1959) law $\psi(t) \propto \rho_{\rm gas}^k$ with $\rho_{\rm gas}$ being the volume gas density.

Other suggestions concern the star formation induced by spiral density waves (e.g., Boissier and Prantzos (1999)) with expressions like:

$$\psi(t) = \nu V(R) R^{-1} \sigma_{\rm gas}^{1.5}, \tag{2.9}$$

with $V(R)$ being the rotational velocity and R the galactocentric distance, or:

$$\psi(t) = 0.017 \Omega_{\rm gas}\sigma_{\rm gas} \propto R^{-1}\sigma_{\rm gas}, \tag{2.10}$$

with $\Omega_{\rm gas}$ being the angular rotation speed of gas (Kennicutt 1998a). It is worth noting that also this law, besides law (2.6), provides a good fit to the data of Fig. 2.1.

2.1.2.2 The Initial Mass Function

The most common parametrizations of the IMF are either a one-slope ($x = 1.35$; Salpeter (1955)) or a multi-slope power law. The most simple example of a one-slope power law is:

$$\varphi(m) = a m^{-(1+x)}, \tag{2.11}$$

generally defined in a mass range of 0.1–100 $M_\odot$, where a is the normalization constant derived by imposing that $\int_{0.1}^{100} m\varphi(m)\mathrm{d}m = 1$.

The multi-slope IMFs were derived from stellar counts in the solar vicinity and suggest a three-slope function. A typical example of a three-slope IMF is that suggested by Kroupa et al. (1993):

$$\begin{aligned} x_1 &= 0.2 \;\; for \;\; M \leq 0.5 M_\odot \\ x_2 &= 1.2 \;\; for \;\; 0.5 < M/M_\odot \leq 1.0 \\ x_3 &= 1.7 \;\; for \;\; M > 1.0 M_\odot \end{aligned} \tag{2.12}$$

Unfortunately, the same analysis cannot be performed in other galaxies and we cannot test if the IMF is the same everywhere. Kroupa (2001) suggested that the IMF in stellar clusters is a universal one, very similar to the Salpeter IMF for stars with masses larger than $0.5 M_\odot$. In particular, this universal IMF (UIMF) should have:

$$\begin{aligned} x_1 &= 0.3 \;\; for \;\; 0.08 \leq M/M_\odot \leq 0.50 \\ x_2 &= 1.3 \;\; for \;\; M > 0.5 M_\odot \end{aligned} \tag{2.13}$$

However, Weidner and Kroupa (2005) suggested that the IMF integrated over galaxies, which controls the distribution of stellar remnants, the number of SNe and the chemical enrichment of a galaxy is generally different from the IMF in stellar clusters. This "galaxial" IMF is given by the integral of the stellar IMF over the embedded star cluster mass function which varies from galaxy to galaxy. Therefore, we should expect that the chemical enrichment histories of different galaxies cannot be reproduced by a unique invariant Salpeter-like IMF. In any case, this galaxial IMF (IGIMF) is always steeper than the universal IMF in the range of massive stars:

$$\begin{aligned} x_1 &= 0.3 \;\; for \;\; 0.08 \leq M/M_\odot \leq 0.50 \\ x_2 &= 1.3 \;\; for \;\; 0.5 < M/M_\odot \leq 1 \\ x_3 &= 1.7 \;\; for \;\; M > 1 M_\odot. \end{aligned} \tag{2.14}$$

As one can see, the UIMF predicts a much larger number of massive stars than Salpeter (1995) and Kroupa et al. (1993) IMFs, and this will produce a large increase in metallicity that should be tested in single cases.

Finally, Chabrier (2003) suggested a log-normal form for the low-mass part of the IMF ($m < 1M_{\odot}$):

$$\varphi(\log m) \propto \mathrm{e}^{-(\log m - \log m_{\mathrm{C}})^2/2\sigma^2} \quad for \;\; M \leq 1M_{\odot}, \tag{2.15}$$

and:

$$\varphi(m) \propto m^{-(1.3\pm0.3)} \quad for \;\; M > 1M_{\odot}, \tag{2.16}$$

where $x = 1.3$ is practically the Salpeter index and $m_{\mathrm{C}} = 0.079M_{\odot}$ and $\sigma = 0.69$ well-characterize the IMF of single stars in the Milky Way.

Derivation of the IMF

We define the current mass distribution of local main sequence (MS) stars as the present day mass function (PDMF), $n(m)$. Let us suppose that we know $n(m)$ from observations. The PDMF, in fact, is derived by the stellar luminosity function of MS stars after applying the mass-luminosity relation. Then, the quantity $n(m)$ can be expressed as follows: for stars with initial masses in the range 0.1–1.0 $M_{\odot}$, which have lifetimes larger than a Hubble time, we can write:

$$n(m) = \int_0^{t_{\mathrm{G}}} \varphi(m)\psi(t)\mathrm{d}t, \tag{2.17}$$

where $t_{\mathrm{G}} = 14\,\mathrm{Gyr}$ (the age of the Universe). The IMF, $\varphi(m)$, can be taken out of the integral if assumed to be constant in time, and the PDMF becomes:

$$n(m) = \varphi(m)\langle\psi\rangle t_{\mathrm{G}}, \tag{2.18}$$

where $\langle\psi\rangle$ is the average SFR in the past.

For stars with lifetimes negligible relative to the age of the Universe, namely, for all the stars with $m > 2M_{\odot}$, we can write instead:

$$n(m) = \int_{t_{\mathrm{G}}-\tau_m}^{t_{\mathrm{G}}} \varphi(m)\psi(t)\mathrm{d}t, \tag{2.19}$$

where τ_m is the lifetime of a star of mass m. Again, if we assume that the IMF is constant in time we can write:

$$n(m) = \varphi(m)\psi(t_{\mathrm{G}})\tau_m, \tag{2.20}$$

having assumed that the SFR did not change during the time interval between $(t_{\mathrm{G}} - \tau_m)$ and t_{G}. The quantity $\psi(t_{\mathrm{G}})$ is the SFR at the present time. Unfortunately, we cannot derive the IMF between 1 and 2 $M_{\odot}$ because none of the previous simplifying hypotheses can be applied. Therefore, the IMF in this mass range will depend on the quantity $b(t_{\mathrm{G}})$, namely, the ratio between the present time SFR and the average SFR in the past:

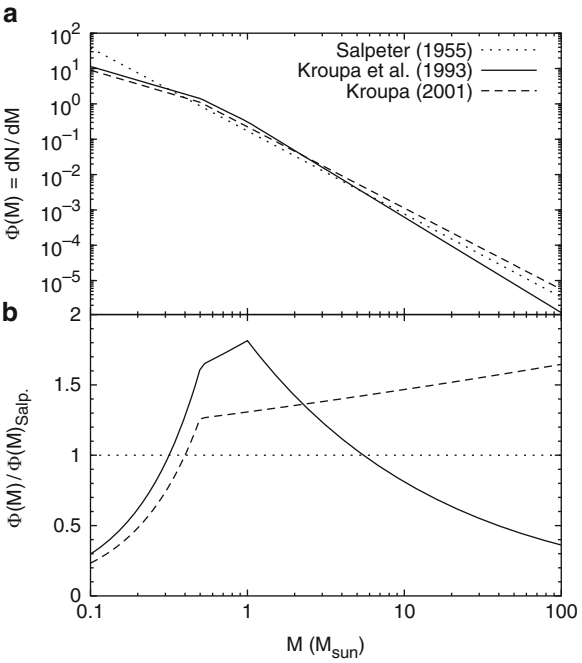

Fig. 2.2 *Upper panel* (**a**): different IMFs. *Lower panel* (**b**): normalization of the multi-slope IMFs to the Salpeter IMF. Figure from Munoz-Mateos et al. (2011); reproduced by kind permission of J. Munoz-Mateos

$$b(t_{\rm G}) = \frac{\psi(t_{\rm G})}{\langle\psi\rangle}. \tag{2.21}$$

This parameter is chosen in order to best fit the two branches of the IMF in the solar vicinity. By following such a procedure, Scalo (1986) found:

$$0.5 \leq b(t_{\rm G}) \leq 1.5 \tag{2.22}$$

in order to derive the IMF in the solar vicinity. This means that the SFR in the solar vicinity did not change more than a factor of two during the disk lifetime, and represents an important constraint to model galactic evolution.

In Fig. 2.2, we show the differences between a single-slope IMF and multi-slope IMFs, which are preferred according to the last studies concerning the solar neighborhood stars.

Derivation of the Star Formation Rate

In order to derive the present time SFR at different galactocentric distances in the Galaxy and in external galaxies, one should use different tracers. Most direct tracers

of SFR in galaxies are sensitive only to the luminosities of massive stars, above 5–10 $M_\odot$. Unfortunately, for typical IMFs these massive stars represent only 5–20% of the total mass of the stellar population, so deriving a total SFR involves a large (factor 5–20) extrapolation over the stellar component which is actually observed.

The most common tracers of star formation are:

- Counts of the supergiants which are luminous enough to be seen also in nearby galaxies under the assumption that their number is proportional to the SFR.
- Otherwise one can measure the H_α and H_β flux from HII regions, which are ionized by young and hot stars, and assume that such a flux is proportional to the SFR. In Kennicutt (1998b), where the reader can find an exhaustive review on the derivation of the SFR in galaxies, the following relation for the total SFR is suggested:

$$\mathrm{SFR}(M_\odot\ \mathrm{yr}^{-1}) = 7.9 \cdot 10^{-42} L_{\mathrm{H}_\alpha}[\mathrm{ergs\,s}^{-1}], \tag{2.23}$$

  measured in a sample of field spiral and irregular galaxies, after adopting the Salpeter IMF over the mass range 0.1–100 $M_\odot$, and the same IMF parametrization is used in all the following tracers.
- The SFR can also be traced by the forbidden lines, in particular by the [OII] luminosity emitted by HII regions: this method has been used to trace star formation in blue irregular galaxies. A suitable calibration is:

$$\mathrm{SFR}(M_\odot\ \mathrm{yr}^{-1}) = (1.4 \pm 0.4) \cdot 10^{-41} L[\mathrm{OII}][\mathrm{ergs\,s}^{-1}]. \tag{2.24}$$

  However, the SFRs derived in this way are less precise than those from H_α because the mean [OII]/H_α ratios vary considerably in individual galaxies.
- The UV continuum luminosity is also often used as a tracer of star formation (see GALEX, galaxy evolution explorer). In this case the conversion between the UV flux and the SFR can be derived by using population synthesis models. The suggested calibration in the wavelength range (1,500–2,800 $\mathring{A}$) is:

$$\mathrm{SFR}(M_\odot\ \mathrm{yr}^{-1}) = 1.4 \cdot 10^{-28} L_{\mathrm{UV}}[\mathrm{ergs\,s}^{-1}\,\mathrm{Hz}^{-1}]. \tag{2.25}$$

  This equation best applies to galaxies with continuous star formation over timescales of 10^8 years or more; the SFR/L_{UV} is significantly lower in younger populations such as starburst galaxies. A possible warning is also given by the fact that also low mass highly evolved stars such as horizontal branch (HB) stars and post-asymptotic giant branch (AGB) stars can strongly affect the UV continuum in the absence of a starburst (see Greggio and Renzini (1990)).
- The far infrared continuum (star forming regions are surrounded by dust) is also connected to the SFR. This tracer in principle should provide an excellent measure of the SFR in dusty circumstellar starbursts. In fact, a fraction of the UV radiation emitted by massive stars is absorbed by dust grains and re-emitted in the far infrared and radio wavelengths. By assuming continuous bursts of age 10–100 Myr, the calibration between SFR and FIR radiation as suggested by Kennicutt is:

$$\mathrm{SFR}(M_\odot\ \mathrm{yr}^{-1}) = 4.5 \cdot 10^{-44} L(\mathrm{FIR})[\mathrm{ergs\,s}^{-1}]. \tag{2.26}$$

- For the radio luminosities we can write (Schmitt et al. 2006):

$$\mathrm{SFR}(M_\odot\ \mathrm{yr}^{-1}) = 0.62 \cdot 10^{-28} L_{1.4\,\mathrm{GHz}}[\mathrm{ergs\,s}^{-1}\,\mathrm{Hz}^{-1}]. \tag{2.27}$$

- The X-ray emission is also a tracer of the SFR, through the X-ray luminosity produced by high-mass X-ray binaries (HMXB). One calibration to derive the SFR in the energy range 2–10 keV and derived from ASCA and BeppoSAX data is (Persic and Rephaeli 2003):

$$\mathrm{SFR}(M_\odot\ \mathrm{yr}^{-1}) = 2.6 \cdot 10^{-40} L_{2-10\,\mathrm{keV}}[\mathrm{ergs\,s}^{-1}]. \tag{2.28}$$

  In the case of X-ray luminosity, a possible source of contamination is the presence of an active galactic nuclei (AGN) in the observed galaxy. In addition, to derive the SFR one should subtract from the X-ray luminosity the contribution of the low-mass X-ray binaries (LMXB).
- Finally, the frequency of Type II supernovae as well as the distribution of SN remnants have also been used as tracers of star formation.

The present time SFR in our Galaxy is derived by adopting some of the tracers discussed above after the assumption of an IMF. Alternatively, the procedure to follow is to assume an IMF and then integrate the equations, which give the PDMF with respect to the mass. In particular, Güsten and Mezger (1982) summarized these kinds of estimates of the present time local SFR and suggested:

$$\psi(t_\mathrm{G}) \sim 2 - 10 M_\odot\ \mathrm{pc}^{-2}\ \mathrm{Gyr}^{-1}. \tag{2.29}$$

The Cosmic SFR

The comoving space density of the global SFR is known as "cosmic SFR" (CSFR) and it has been measured up to high redshift by means of the comoving luminosity density in various wavelength bands. The physical meaning of the CSFR is of cumulative SFR owing to galaxies of different morphological types present in a unitary comoving volume of the Universe. In fact, at high redshift, we cannot distinguish galaxy morphology but only trace the luminosity density of galaxies. The first measure of the comoving luminosity density of the Universe was done in three wavebands (2,800 Å, 4,400 Å, and 1 μm) over the redshift range $0 < z < 1$ by Lilly et al. (1996). They found that the comoving luminosity density is increasing markedly with redshift for all the studied wavebands. As a consequence of this, also the CSFR is increasing with redshift up to $z = 1$. In the following years, many studies on the derivation of the CSFR have appeared, and at present data have been collected up to very high redshift, although the data for $z > 1$ are still uncertain and

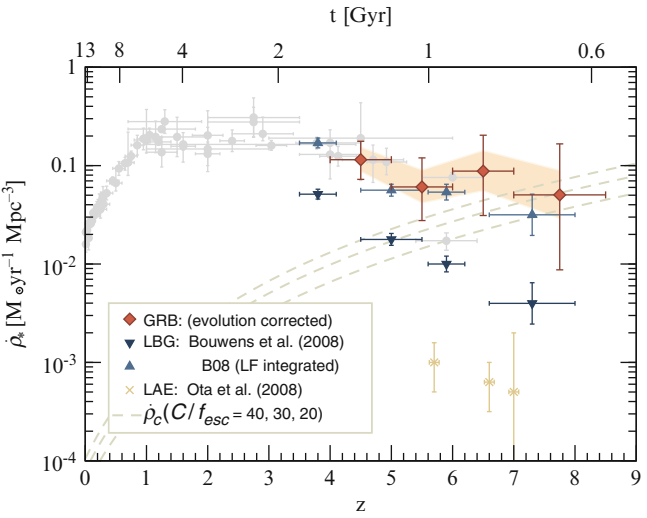

Fig. 2.3 The cosmic star formation history. Shown are the data compiled in Hopkins and Beacom (2006) (*light circles*) and contributions from Lyα emitters (LAE, Ota et al. 2008). Lyman-break galaxies data are shown for two UV luminosity function integrations: down to $0.2L^*_{z=3}$ (*down triangles*; as given in Bouwens et al. (2008)) and complete (*up triangles*), Swift GRB inferred rates are indicated by diamonds with the *shaded band* showing the uncertainties of the modeling. Also shown is the critical $\dot{\rho}_*$ from Madau et al. (1998) for $C/f_{\rm esc} = 40$, 30, and 20 (*dashed lines*: *top* to *bottom*, $f_{\rm esc}$ is the fractions of photons escaping their galaxy and C is the clumpiness of the ISM). Figure from Kistler et al. (2009); reproduced by kind permission of M.D. Kistler

one of the most important uncertainties is represented by dust extinction at very high redshift. In order to derive the CSFR from luminosity densities, one has to assume star formation calibrations, as discussed above. The tracers used to derive the CSFR have been the H_α, H_β, [OII], UV, and FIR luminosities. Recently, the CSFR has been measured also from gamma-ray burst (GRB) counts and extended up to $z \sim 8$, which corresponds to the estimated redshift of GRB 090423, and it shows no significant decrease of the CSFR. In Fig. 2.3 we show a comparison between various derived CSFR as functions of redshift.

A Threshold in the Star Formation

Originally, Kennicutt (1989) and other later studies had indicated the existence of a star formation threshold in the interstellar gas density, below which star formation stops. This was suggested by a clear truncation observed in the H_α profiles of star forming galaxies. From a theoretical point of view, a sudden decrease in star formation at low gas densities is expected from simple gravitational stability considerations. Below a critical density, the gas disk is stable against the growth of large-scale density perturbations. As a consequence, one would expect

cloud growth and star formation to be suppressed. Later on, GALEX studies (Boissier et al. 2007) had pointed out that the UV radial profiles in galactic disks, interpreted as star formation, do not show a sharp truncation. A more recent paper (Goddard et al. 2010) suggests that some galaxies show H_α truncation and no UV truncation, while others show no threshold in either H_α or UV and have a gradually declining surface brightness. Therefore, the situation is still unclear suggesting that in some disks, star formation extends beyond the main optical radius (r_{25}).[1] Some chemical evolution models have adopted a threshold in the gas density for star formation and this has important consequences on chemical evolution such as on the predicted abundance gradients along galactic disks (see Chap. 5).

2.1.3 The Stellar Yields

The stellar yields, namely, the amount of both newly formed and pre-existing elements ejected by stars of all masses at their death, represent a fundamental ingredient to compute galactic chemical evolution. They can be calculated by knowing stellar evolution and nucleosynthesis.

All the elements with mass number A from 12 to 60 have been formed in stars during the quiescent burnings in stellar evolution. Stars transform H into He and then He into heavier atoms until the Fe-peak elements, where the binding energy per nucleon reaches a maximum and the nuclear fusion reactions stop. H is transformed into He through the proton–proton chain or the CNO-cycle according to the stellar mass, then ^{4}He is transformed into ^{12}C through the triple-α reaction. Elements heavier than ^{12}C are then produced by synthesis of α-particles: they are called α-elements (O, Ne, Mg, Si, S, and Ca). The last main burning in stars is the ^{28}Si -burning, which produces ^{56}Ni, which then β-decays into ^{56}Co and ^{56}Fe. Si-burning can be quiescent or explosive (depending on the temperature). Explosive nucleosynthesis occurring during supernova explosions mainly produces Fe-peak elements. Elements originating from s- and r-processes (with $A > 60$ up to Th and U) are formed by means of slow (s) or rapid (r) (relative to the timescale of the β-decay process) neutron capture by Fe and other heavy seed nuclei; s-processing occurs during quiescent He-burning, whereas r-processing occurs during SN II explosions (explosive nucleosynthesis).

Stars of different masses produce different chemical elements and we recall here the various stellar mass ranges and their nucleosynthesis products. In particular:

- *Brown dwarfs.* Stars with masses $M < 0.1 M_\odot$ which never ignite H. They do not enrich the ISM in chemical elements but only lockup gas.
- *Low and intermediate mass stars* ($0.8 \leq M/M_\odot \leq M_{\rm up}$). The mass $M_{\rm up}$ is defined as the limiting mass for the formation of a fully degenerate C–O core and

[1] The radius corresponding to a surface brightness of 25 magnitudes per arcsec in the blue band.

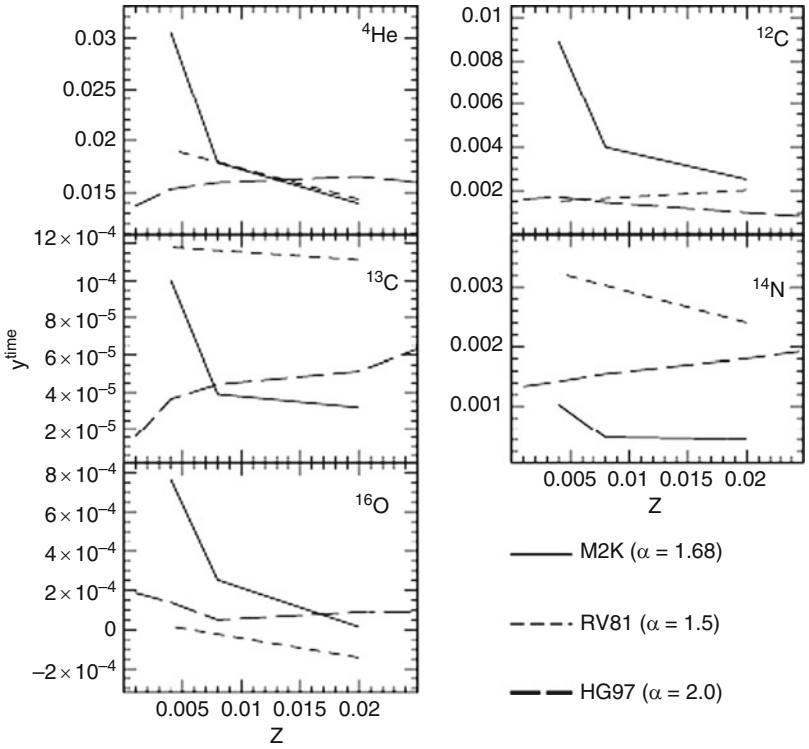

Fig. 2.4 The yields integrated over the Salpeter (1955) IMF of He, C, and N produced by low and intermediate mass stars as functions of the initial stellar metallicity. Different results are compared here: those of RV81 (Renzini and Voli 1981), those of HG97 (van den Hoek and Groenewegen 1997) and those of M2K (Marigo 2001). The mixing length parameters (α) adopted by the authors are indicated. Figure from Marigo (2001)

its value ($\sim$6–8$M_\odot$) depends on the treatment of convection. These stars produce mainly ^{4}He, ^{12}C, and ^{14}N plus some CNO isotopes and heavy s-process ($A > 90$) elements. In Fig. 2.4, we show a compilation of yields from low and intermediate mass stars. The yields differ by the different adopted physical inputs such as the mixing-length parameter which controls the process of convection.

- *Massive stars* ($M_{\rm up} < M/M_\odot \leq M_{\rm WR}$). In the mass range 8–10$M_\odot$, stars explode as e-capture supernovae. Electron capture triggers instability in the stars and at the same time O ignites explosively in the O–Ne–Mg degenerate core. In the mass range $10 - M_{\rm WR}$, where $M_{\rm WR}$ is the minimum mass for the formation of a Wolf–Rayet star and is rather uncertain, since it depends on the stellar mass loss, which in turn depends on the initial stellar mass and metallicity (for a solar chemical composition $M_{\rm WR} \sim 25M_\odot$), the stars end their life as Type II SNe and explode by core-collapse. Also uncertain is the amount of the ejected material which falls back on the contracting core during the explosion and consequently the formation of a black hole rather than a neutron star. These stars produce

mainly α-elements, some N, some Fe-peak elements, light s-process elements ($A < 90$) and perhaps r-process elements. Stars more massive than M_{WR} should end up as Type Ib/c SNe; they are also core-collapse SNe and are linked to the GRBs. Some of these massive SNe are particularly energetic ($E_0 = 10^{52}$ ergs, with E_0 being the initial blast wave energy) and for this reason they have been called "hypernovae."

- *Type Ia SNe* (white dwarfs (WDs) in binary systems, see later). They produce mainly Fe-peak elements and traces of elements from C to Si.
- *Very massive objects* ($M > 100 M_{\odot}$). The most recent calculations suggest that they should produce mainly oxygen, although many uncertainties are still present.

In Figs. 2.5–2.10, we show a comparison between stellar yields from massive stars computed for different initial stellar metallicities and with different assumptions concerning the mass loss. In particular, some yields are obtained by assuming mass loss by stellar winds with a strong dependence on metallicity, whereas others are computed by means of conservative models without mass loss. One important difference arises for oxygen in massive stars for solar and above solar metallicities and mass loss: in this case, the O yield is strongly depressed as a consequence of mass loss. In fact, the stars with masses $>25 M_{\odot}$ and solar and above solar metallicity lose a large amount of matter rich of He and C, thus subtracting those elements to further processing which would eventually lead to O and heavier elements. So the net effect of mass loss is to increase the production of He and C and to depress that of oxygen (see Fig. 2.10). More recently, Meynet and Maeder (2002, 2003, 2005) have computed a grid of models for stars with $M > 20 M_{\odot}$ including rotation and metallicity dependent mass loss. The effect of metallicity dependent mass loss in decreasing the O production in massive stars was confirmed, although they employed significantly lower mass loss rates compared with Maeder (1992). With these models, they were able to reproduce the frequency of WR stars and the observed WN/WC ratio, as it was the case for the previous Maeder results. Therefore, it appears that the earlier mass loss rates made-up for the omission of rotation in the stellar models. On the other hand, the dependence upon metallicities of the yields computed with conservative stellar models is generally not very strong except perhaps for the yields computed with zero initial stellar metallicity (Pop III stars) and for the yields of Fe.

In Figs. 2.8 and 2.9, we show recent results for conservative stellar models of massive stars at different metallicities. While the O yields are not much dependent upon the initial stellar metallicity, the Fe yields seem to change dramatically with the stellar metallicity.

2.1.3.1 Yields from Population III Stars

In recent years, a great deal of calculations to derive the yields of primordial (no metals) stars has appeared in the literature. It is generally believed that primordial stars should have been very massive. There are several reasons for suggesting

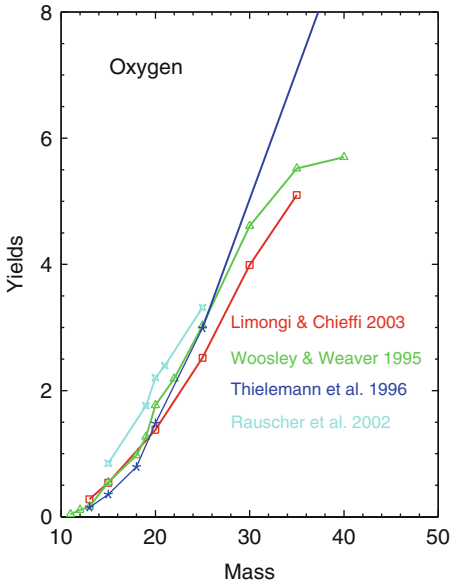

Fig. 2.5 The yields of oxygen for massive stars as computed by several authors, as indicated in the figure. None of these calculations takes into account mass loss by stellar wind. The yields refer to the solar chemical composition

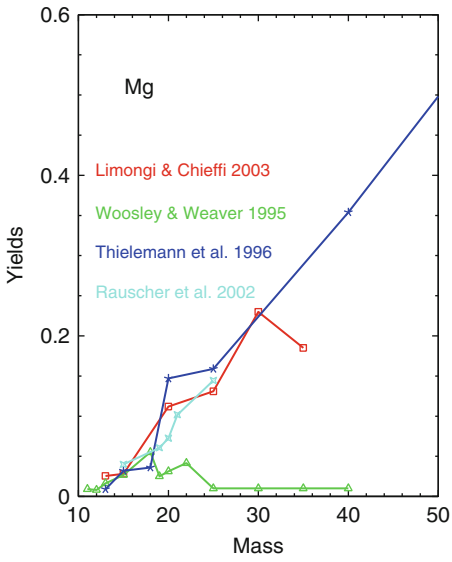

Fig. 2.6 Same as Fig. 2.5 for magnesium

that the first stars were more massive than today stars. The Jeans mass, i.e., the minimum mass necessary for a gas cloud to collapse under its self-gravity scales as $T^{3/2}$ with an even steeper dependence on the temperature if turbulent phenomena are taken into account. Metals are indeed the most effective coolants in gas and their presence permits the formation of low mass stars. In the absence of metals, as it was in the primordial gas, the cooling was due to the rotational-vibrational

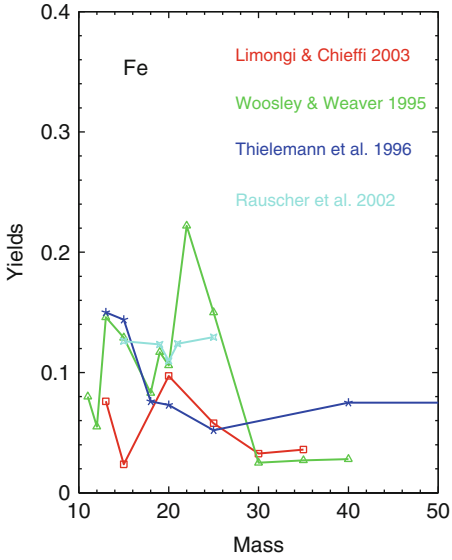

Fig. 2.7 Same as Figs. 2.5 and 2.6 for Fe

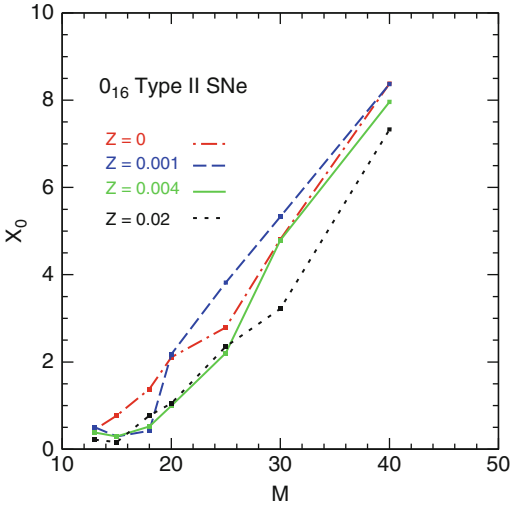

Fig. 2.8 The O yields as calculated by Nomoto et al. (2006) for different metallicities. These calculations do not take into account mass loss by stellar wind

transitions of molecular hydrogen. Hydrodynamical simulations of the collapse and fragmentation of primordial gas clouds suggest that the very first stars should have had masses larger than $100 M_{\odot}$. However, the high mass biased star formation must have lasted until the metallicity of the ISM reached a critical value, at which point the star formation switched into the low mass mode. This critical metallicity has been calculated to be in the range $(10^{-6} - 10^{-4}) Z_{\odot}$ (Schneider et al. 2002). Being so massive, population III stars should start their MS phase burning H by means of the CNO reaction chain, but since they lack CNO elements, they are forced to burn H via the $p - p$ chain. However, the $p - p$ chain is not so effective in

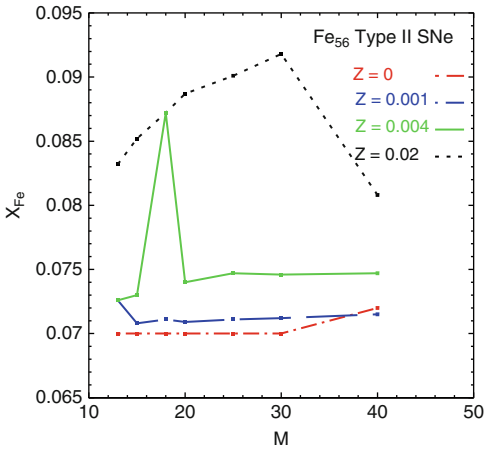

Fig. 2.9 Same as Fig. 2.8 for Fe

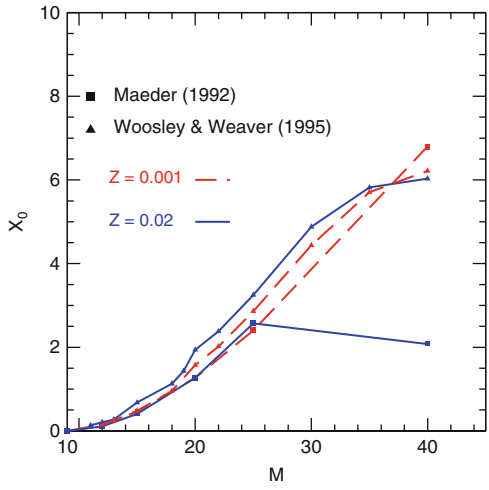

Fig. 2.10 The effect of metallicity dependent mass loss on the oxygen yield. The comparison is between the conservative yields of Woosley and Weaver (1995) for $Z = 0.001$ and $Z = 0.02$ and the yields with mass loss of Maeder (1992) for the same metallicity. As one can see, the effect of mass loss for a solar metallicity is a quite important one

producing the energy necessary to counterbalance their gravity; therefore, the stars are forced to contract and increase their central temperature until the 3α reaction starts and creates some ^{12}C; at this point, they can start burning H via the CNO-cycle. Owing to the lack of metals, these stars suffer less mass loss than the normal stars belonging to populations II and I. As a consequence, they end their lives by creating a black hole in the center and explode as pair-creation supernovae, in other words, the explosion is triggered by the formation of couples of e^+ and e^- which destabilize the star. These SNe leave no remnant. Clearly the nucleosynthesis products of these population III stars are different from the products of population II/I stars. The nucleosynthesis of zero-metal massive stars was computed since the early eighties (Ober et al. 1983; El Eid et al. 1983) and the work on this field has continued until very recently (e.g., Heger and Woosley (2010)). One interesting aspect of these massive Pop III stars is that they can produce some primary nitrogen

and thus perhaps explain the high [N/O] ratio found in very metal poor halo stars, although very metal poor ($Z = 10^{-8}$) rotating normal massive stars can also produce primary nitrogen (Chiappini et al. (2006) and Chap. 5). Moreover, it has been suggested that Pop III stars could explain some of the peculiar behaviors of Fe-peak elements (Mn, Co, Cr, Ni, and Zn) at low metallicity (see Umeda and Nomoto (2005)). One interesting aspect of this population III is that only a few of these stars must have existed, since the increase of metallicity to the threshold value must have happened very quickly. Therefore, it is not clear whether these massive zero-metal stars have had a real impact on the abundance patterns that we see in very metal poor stars. Unfortunately, the situation at present is such that we cannot prove or disprove the existence of zero-metal stars on the basis of the available data on very metal poor stars.

The most metal poor stars have been found in the halo of our Galaxy and they can be distinguished into four classes: the ultra metal poor stars with [Fe/H] < -4.0 dex; the extremely metal poor stars with [Fe/H] < -3.0 dex, the metal poor stars with [Fe/H] < -1.0 dex, and the carbon-enhanced metal poor stars (CEMP) with [Fe/H] < -1.0 dex and [C/Fe] > 0.9 dex. The CEMP stars represent a nonnegligible fraction of all metal poor stars; the most metal poor CEMP star known so far is HE 1327-2326 with a [Fe/H] ~ -5.96 dex (Frebel et al. 2008). The majority of CEMP show also overabundances of N and O and heavy s-process elements, difficult to reconcile with standard nucleosynthesis in massive stars. Since most of CEMP stars have been found to be spectroscopic binaries, the most simple explanation of their anomalous abundances is accretion from an AGB companion. In principle, the abundance ratios in CEMP stars can be also the result of the pollution of the interstellar medium by the first zero-metal stars. Comparison between the anomalous abundance ratios of the most metal poor CEMP stars with the yields predicted for population III stars could be then used to impose constraints on the masses and explosion energies of metal free supernovae.

2.1.3.2 Type II SN Progenitors

Originally, the SNe were classified into two main types (I and II) on the basis of the presence (Type II) or absence (Type I) of H lines in their spectra (Zwicky 1938). At the present time, we distinguish among several SN II types on the basis of the spectra obtained at maximum light. Classical Type II SNe have prominent Balmer lines exhibiting P-Cygni profiles and represent about 70% of the exploding stars in the Universe. The classification can be further subdivided into Types II-L and II-P, according to the shape of the light curve which can be linear (L) or have a plateau (P). Then, Type IIdw SNe have strong H lines in emission. They can be distinguished from the classical Type II SNe by the lack of absorption in their Balmer lines. This definition reflects the fact that these SNe undergo significant interaction with a "dense wind" produced by the SN progenitor prior to explosion (Chugai 1997). As we have already said, the mechanism for the explosion of SNe II is the core-collapse: the basic idea is that there should be a core bounce giving

rise to the ejection of the external mantle. This bounce is due to the fact that the Fe-core is contracting and when its density reaches the density of the nuclei of the atoms ($\simeq 2 \cdot 10^{14}\,\mathrm{g\,cm^{-3}}$) the matter becomes incompressible and the collapse halts abruptly thus giving rise to the bounce. The bounce, in turn, produces pressure waves propagating towards the external parts. Such waves then become a shock wave with an energy equal to the gravitational energy of the collapse. The main problem for the explosion of these stars is that the energy produced by the explosion should be sufficient to heat the mantle of the star and eject it. Unfortunately, the enormous energy in the shock wave after the core bounce is largely used to photo-disintegrate the outer core layers consisting of iron and is also lost through the neutrino escaping from the hot core behind the shock during the neutronization process (at very high density a proton in the nucleus captures an electron and form a neutron plus a neutrino). Therefore, only a small fraction of the explosion energy is eventually available to heat the mantle, especially if the mass of the core is large. As a consequence, the shock wave, when it reaches the most external regions, has lost most of its energy and dies. Bethe and Wilson (1985) proposed a mechanism which allows the shock wave to rejuvenate and give rise to a *delayed explosion*. The rejuvenation is due to a small fraction of the neutrino energy equal to the total gravitational binding energy of the neutron star of 10^{53} erg, which can be trapped in the very dense matter and give the shock wave the strength to eject the mantle. Type II SNe leaves a neutron star or a black hole after the explosion, according to the mass of their core.

2.1.3.3 Type Ib/c Supernovae and Gamma-Ray Bursts

Gamma-Ray Bursts (GRBs) are sudden and powerful flashes of gamma-ray radiation, occurring random by a rate of $\sim$1 per day in the Universe. The duration of GRBs at MeV energies ranges from 10^{-3} s to about 10^{3} s, with long bursts being characterized by a duration >2 s. During the last few years, it has been established that at least a large fraction of long-duration GRBs is directly connected with the death of massive stars. This scenario has got strong support from observations of SN features in the spectra of several of GRB afterglows. Examples of the spectroscopic SN/GRB connection include SN1998bw/GRB980425, SN2003dh/GRB030329, SN2003lw/GRB031203, and SN2006aj/GRB060218. Type Ib SNe are identified by spectra with no evident Balmer lines, weak or absent Si II lines and strong He I lines. Bertola (1964) reported the first observation of this class of SNe, but the "Ib" designation was introduced later by Elias et al. (1985). Type Ic SNe are characterized by weak or absent H and He lines and no evident Si II. They show Ca II H&K in absorption, the Ca II near-IR triplet with a P-Cygni profile, and O I in absorption. The "Ic" class was introduced by Wheeler and Harkness (1986). The SNe Ib/c can originate either from single Wolf–Rayet stars (stars with $M > M_{\mathrm{WR}}$ which have lost most of their envelope) or from massive stars in binary systems. In the latter case, the suggested mass range is $12 < M/M_{\odot} < 20$ (Baron 1992). Very probably both kinds of progenitors are necessary, in particular because Wolf–Rayet

stars are very few if the IMF is a normal Salpeter-like one, and therefore are probably not enough to reproduce the present time observed Type Ib/c SN rate in galaxies. The SNe Ib/c explode also by core-collapse and depending on the amount of mass lost they can leave a neutron star or a black hole. Detailed stellar calculations (e.g., Georgy et al. (2009)) suggest that $M_{\rm WR}$ strongly depends on the mass loss rate and since the mass loss rate is a function of metallicity, the value of $M_{\rm WR}$ increases with decreasing metallicity. In other words, to have a Wolf–Rayet star, namely, a star which has lost all its H and He envelope, the mass lost during the stellar lifetime must have been large and this happens more easily at high metallicity.

Because of the association with long GRBs, it is reasonable to think that a fraction of Type Ib/c SNe can give rise to GRBs. Among the proposed models to explain the GRBs, the "collapsar" model (e.g., MacFadyen and Woosley (1999)) suggests that a Wolf–Rayet progenitor undergoes core-collapse, producing a rapidly rotating black hole surrounded by an accretion disk which injects energy into the system and thus acts as a "central engine." The energy extracted from this system supports a quasi-spherical Type Ib/c SN explosion and drives collimated jets through the stellar rotation axis which produce the prompt gamma-ray and afterglow emission.

2.1.3.4 Type Ia SN Progenitors

Type Ia SNe are characterized by the lack of H lines and by a strong absorption observed at $\lambda\lambda$ 6,347, 6,371 Å attributed to the P-Cyg profile of Si II. There is a general consensus about the fact that SNe Ia originate from C-deflagration in C–O WDs in binary systems, but several evolutionary paths can lead to such an event.

Two main evolutionary scenarios for the progenitors of Type Ia SNe have been proposed:

- Single degenerate (SD) scenario (see Fig. 2.11): The classical scenario of Whelan and Iben (1973), namely, C-deflagration in a C–O WD reaching the Chandrasekhar mass, $M_{\rm Ch} \sim 1.44 M_{\odot}$, after accreting material from a red giant companion. One of the limitations of this scenario is that the accretion rate should be defined in a quite narrow range of values. To avoid this problem, it was proposed a similar scenario (see Fig. 2.12), where the companion can be either a red giant or a main sequence star, including a metallicity effect which suggests that no Type Ia systems can form for [Fe/H]< -1.0 dex. This is due to the development of a strong radiative wind from the C–O WD, which stabilizes the accretion from the companion, allowing for larger mass accretion rates than in the previous scenario. The clock to the explosion in the classic SD scenario is given by the lifetime of the secondary star in the binary system where the WD is the primary star (the originally more massive one). Therefore, the largest mass for a secondary is $8 M_{\odot}$, which is the maximum mass for the formation of a C–O WD, in classical models of stellar evolution. As a consequence, the

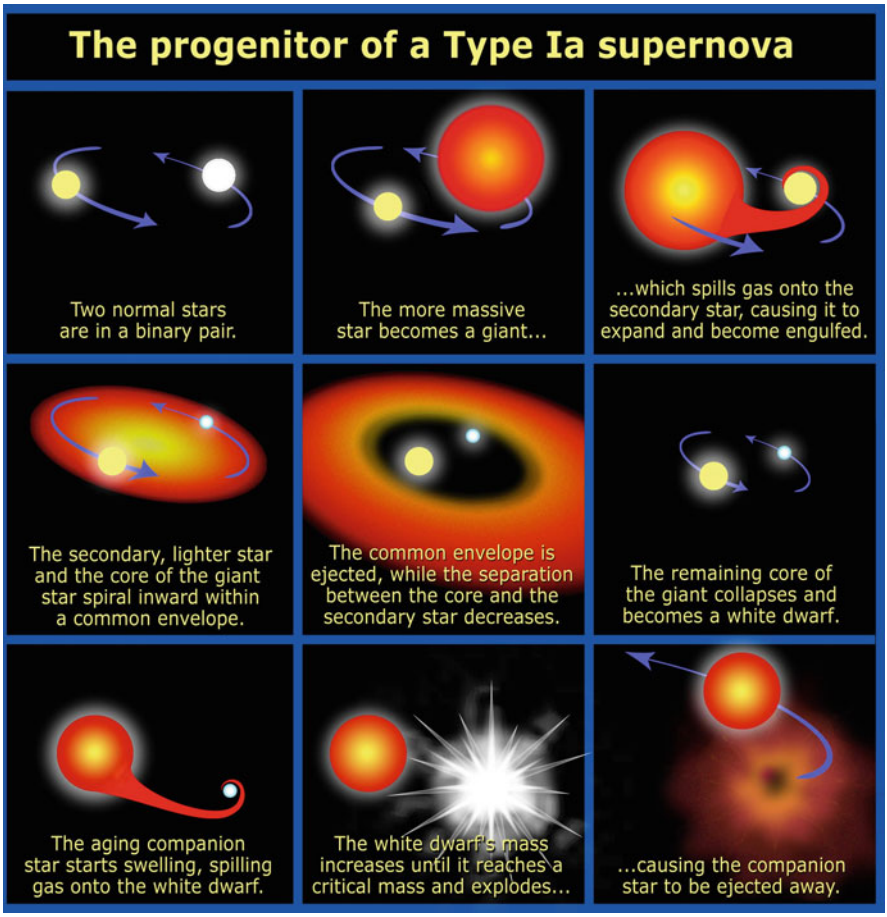

Fig. 2.11 The progenitor of a type Ia SN in the context of the single-degenerate model (Illustration credit: NASA, ESA, and A. Field (STSci))

minimum timescale for the occurrence of Type Ia SNe is ∼30 to 40 Myr (i.e., the lifetime of a $8M_{\odot}$) after the beginning of star formation. The minimum mass for the secondary is $0.8M_{\odot}$ which is the star with lifetime equal to the age of the Universe. This is suggested by the fact that Type Ia SNe are observed in elliptical galaxies which stopped forming stars 10 Gyr ago. Stars with masses below this limit are obviously not considered. In the Hachisu et al. (1999) scenario, the first appearance of SNe Ia is delayed relative to the classic SD scenario; first of all because the gas, out of which the SN Ia progenitors form, has to reach [Fe/H]∼−1.0, and then because the maximum mass for the secondary star is assumed to be 2.3 $M_{\odot}$, which lives much longer than a $8M_{\odot}$ star. In summary, the mass range for both primary and secondary stars is, in principle, between 0.8 and $8M_{\odot}$, although two stars of $0.8M_{\odot}$ are too small to give rise to a WD

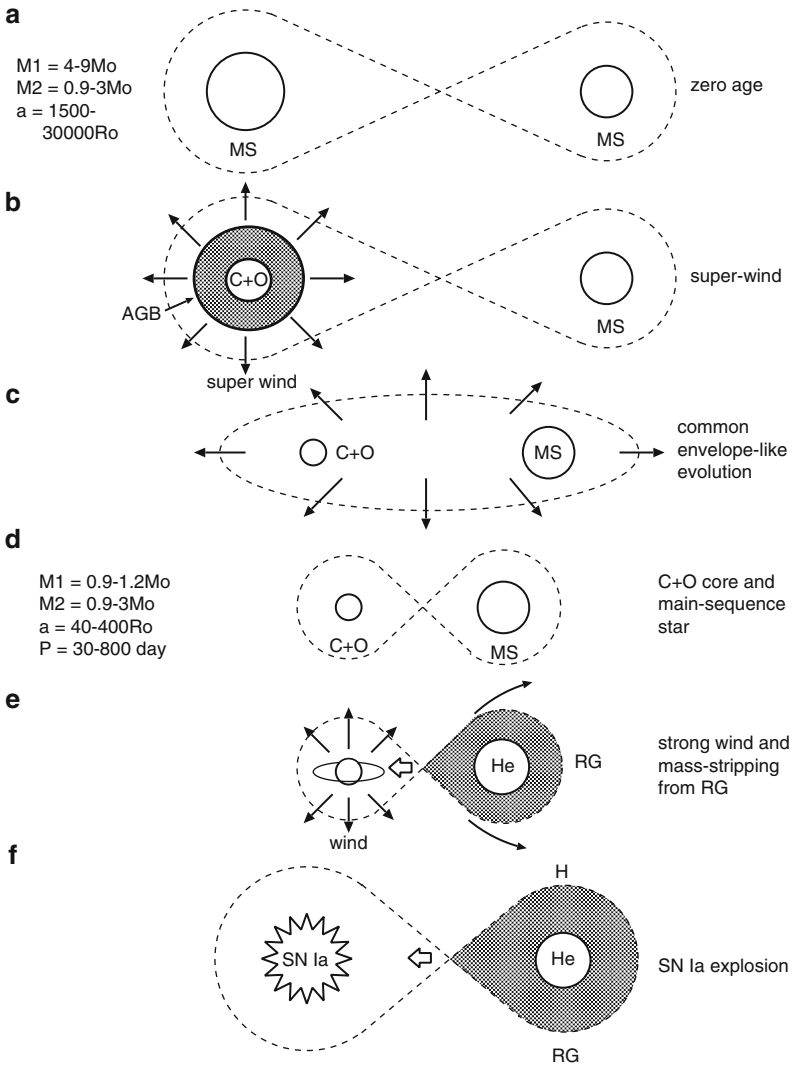

Fig. 2.12 An illustration of the symbiotic channel to Type Ia supernovae (SD scenario). The various phases are labeled a, b, c, d, e and f. Figure from Hachisu et al. (1999); reproduced by kind permission of I. Hachisu

with a Chandrasekhar mass, and therefore the mass of the primary star should be assumed to be high enough to ensure that, even after accretion from a $0.8 M_{\odot}$ star secondary, it will reach the Chandrasekhar mass (Fig. 2.13).

- Double degenerate (DD) scenario: The merging of two C–O WDs, due to loss of angular momentum caused by gravitational wave radiation, which explode by C-deflagration when $M_{\rm Ch}$ is reached (Iben and Tutukov 1984). In this scenario,

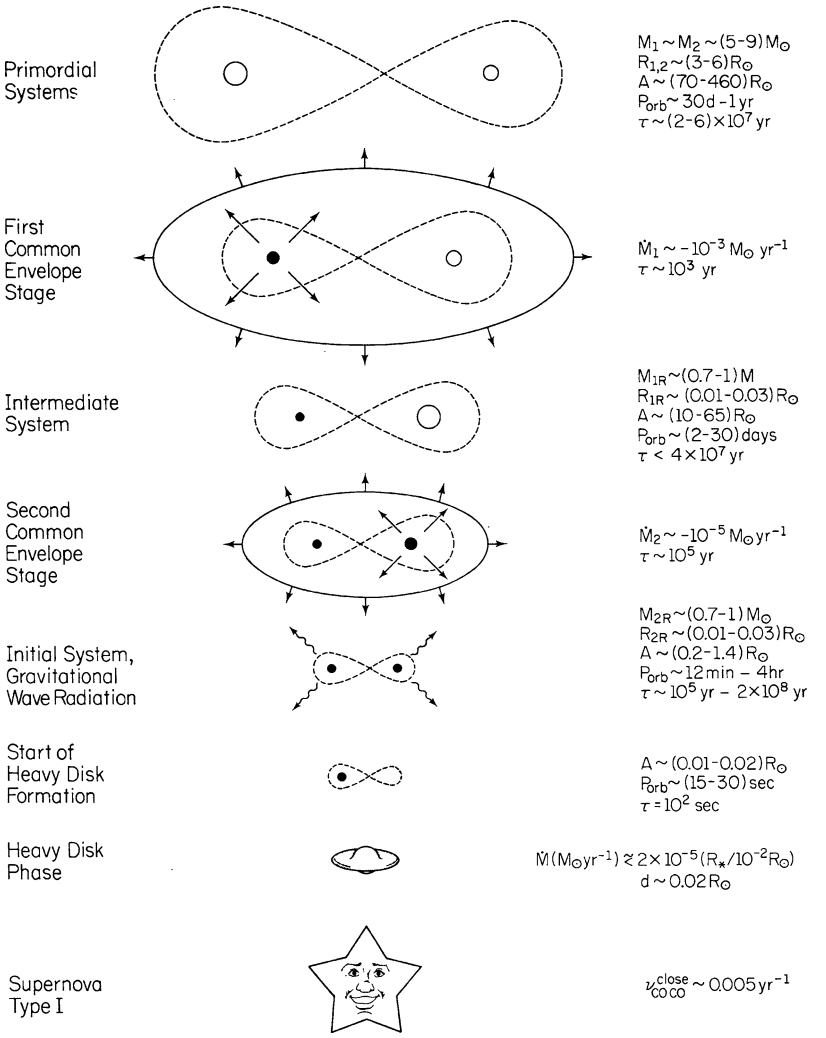

Fig. 2.13 The main stages of the evolution of a primordially close binary system of two WDs merging after loss of angular momentum due to gravitational wave emission. The system evolves through two common envelope phases before the two components become WDs. M_1 and M_2 are the primary and secondary masses, respectively. R_1 and R_2 are the radii of the primary and secondary stars, respectively. R_{1R} and R_{2R} are the radii of the primary and secondary stars after the common envelope phases, respectively. The masses M_{1R} and M_{2R} are the masses after the two common envelope phases of the primary and secondary star, respectively. The quantity A is the separation of the system and τ is the timescale for the various phases. From Iben and Tutukov (1984), Ap. J. Suppl. vol. 54, 335; reproduced by kind permission of I. Iben

the two C–O WDs should be of $\sim 0.7 M_{\odot}$ in order to give rise to a Chandrasekhar mass after they merge; therefore, their progenitors should be in the range (5–8) $M_{\odot}$ (stars of lower masses leave WDs of masses lower than $0.7 M_{\odot}$). The clock to the explosion here is given by the lifetime of the secondary star plus the gravitational time-delay which depends on the original separation of the two WDs. The minimum timescale for the appearance of the first Type Ia SNe in this scenario is, therefore, as low as $\sim$30 to 40 Myr plus the minimum gravitational time-delay ($\sim$1 Myr). For more recent results on the DD scenario see Greggio (2005) and Chap. 4.

Within any scenario, the explosion can occur either when the C–O WD reaches the Chandrasekhar mass and carbon deflagrates at the center or when a massive enough helium layer is accumulated on top of the C–O WD. In this last case, there is He-detonation which induces an off-center carbon deflagration before the Chandrasekhar mass is reached (sub-chandra exploders, e.g., Woosley and Weaver (1994)).

While the chandra-exploders are supposed to produce the same nucleosynthesis (C-deflagration of a Chandrasekhar mass), they predict a different evolution of the Type Ia SN rate and different typical timescales for the SN Ia enrichment, if coupled with different star formation histories in galaxies. A way of defining the typical Type Ia SN timescale is to assume it as the time when the maximum in the Type Ia SN rate is reached. This timescale varies according to the chosen progenitor model and to the assumed star formation history, which in turn varies from galaxy to galaxy. For the solar vicinity, this timescale is at least 1 Gyr, if the SD or DD scenarios are assumed, whereas for elliptical galaxies, where the stars formed much more quickly, this timescale is only $\sim$0.5 Gyr (see next chapters).

Type Ia Supernova Yields

Nomoto et al. (1984) computed a model predicting the nucleosynthesis arising from the C-deflagration of a WD of 1 $M_{\odot}$ after reaching the Chandrasekhar mass limit. This basic model was called W7 and it reproduced almost perfectly the observed abundance pattern in supernovae Ia. The assumed companion of the WD was a red giant star and the rate of accretion onto the WD, $\dot{M} = 4 \cdot 10^{-8} M_{\odot}$ yr^{-1}. The C-deflagration produces explosive nucleosynthesis and roughly 0.58 $M_{\odot}$ of the WD transforms into ^{56}Ni which then decays into ^{56}Co and ^{56}Fe in the most internal layers, whereas the external layers are transformed into elements from Si to C. This model is still the best to represent the nucleosynthesis in a Type Ia supernova. More recently, Iwamoto et al. (1999) revised slightly model W7 and presented several variations of it where the final mass of Fe varies from $0.56 M_{\odot}$ to $0.77 M_{\odot}$ for the same WD mass and slightly different explosion energies. It should be noted, in fact, that a spread in the maximum luminosities of SNe Ia has been observed (Phillips 1993) thus implying different amounts of Fe and challenging the constancy of the amount of ^{56} Ni produced during a SN Ia explosion. The different luminosities

may suggest a dispersion in the progenitor masses, in the sense that in some cases the mass of the exploding WD can be less than $1.4 M_{\odot}$. As a consequence, mechanisms which can lead to the explosion of a sub-chandra mass (0.6–$1.0\, M_{\odot}$) have been proposed. Variations in the explosion mechanism could also produce a dispersion in the absolute magnitudes; besides deflagration, other possible explosion mechanisms are detonation, delayed detonation, pulsating delayed detonation, and tamped-detonation, although C-deflagration is preferred because it produces the right amount of the elements seen in the SN Ia spectra. Finally, differences in the internal composition of the WD, in particular concerning the C/O ratio at the time of explosion, may cause differences in the SN Ia luminosities. This spread in the luminosities challenges the role of standard candles attributed so far to SNe Ia. However, it has been shown that there exist a correlation between the maximum absolute magnitude of SNe Ia and the rate of decline of their luminosity after the maximum; this allows one to calculate the maximum luminosity in any case and, therefore, to retain the SNe Ia as standard candles.

2.1.3.5 Supernova Rates in Galaxies of Different Morphological Types

Type Ia SNe are observed in galaxies of all morphological types whereas Type II and Ib/c SNe only in starforming galaxies. This is because core-collapse SNe (Type II and Ib/c) are originating from massive short living stars, whereas Type Ia SNe, being the outcome of the explosion of a C–O WD, have explosion times ranging from 35 Myr to a Hubble time and, therefore, can be still exploding also in objects where the star formation has stopped several Gyr ago, such as elliptical galaxies. Because of their large range of explosion times, Type Ia SNe have been divided into two categories: *prompt*, namely, those with explosion times ≤ 100 Myr, and *tardy*, all the others with explosion times >100 Myr. Supernova rates are measured in terms of number of SNe per century per $10^{-10} L_{\mathrm{B}_{\odot}}$ (SNu) or per $10^{-10} M_{\odot}$ (SNuM). In Table 2.1, we report the SN rates observed in galaxies of different morphological types.

From Table 2.1, one can see a clear increase of the SN rates per unit mass from E/S0 to Irr for all SN types. The masses of galaxies decrease from E/S0 to Irr as shown in Fig. 2.14. The masses of galaxies are often derived from the observed broad band fluxes by fitting them with spectrophotometric galaxy evolution models. One uncertainty involved into this calculation is the IMF which needs to be assumed.

Table 2.1 Supernova rates in SNuM as functions of galactic morphological type from Mannucci et al. (2005)

Galaxy	Type Ia	Type Ib/c	Type II
E/S0	$0.044^{+0.016}_{-0.014}$	< 0.0093	< 0.013
S0a/b	$0.065^{+0.027}_{-0.025}$	$0.036^{+0.028}_{-0.018}$	$0.012^{+0.069}_{-0.054}$
Sbc/d	$0.17^{+0.068}_{-0.063}$	$0.12^{+0.074}_{-0.059}$	$0.74^{+0.31}_{-0.30}$
Irr	$0.77^{+0.42}_{-0.31}$	$0.54^{+0.66}_{-0.38}$	$1.7^{+1.4}_{-1.0}$

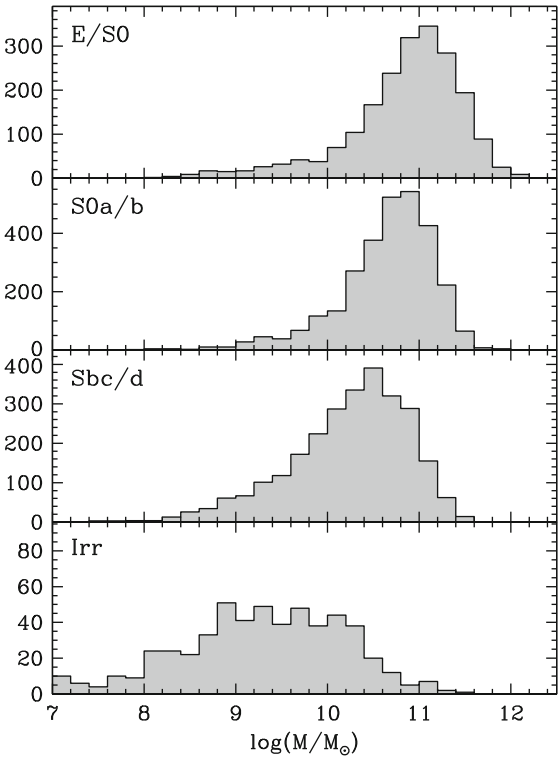

Fig. 2.14 Distribution of galaxy stellar mass for different galactic morphological types. Figure from Mannucci et al. (2005)

However, these methods are expected to give rather accurate results when the redshift and the morphological type of the galaxy are known: for a given IMF, the typical uncertainties in the derived total masses are less than 40%. However, larger uncertainties arise for different IMFs. For example, a factor of two difference in galaxy mass is found passing from a Salpeter (1955) to a Kroupa (2001) IMF. If we assume that the IMF is the same for all galaxies, this uncertainty will only shift up or down the masses along the Hubble sequence; but if the IMF would vary from galaxy to galaxy, then a differential effect in the derivation of the masses would be introduced. The masses of the galaxies in Fig. 2.14 are derived from the K-band luminosity and the B-K color. In fact, there is a correlation between the M/L ratio and the optical to near-infrared colors found by Bell and de Jong (2001) who computed the M/L of galaxies by means of spectrophotometric galactic models.

The SN rates for the Milky Way can be derived from Table 2.1 when a Galactic mass is assumed. More recent studies of the total SN rate, including all SN types, suggested for the Milky Way 2.84 ± 0.60 SNe per century (Li et al. 2011).

2.1.3.6 Nova Progenitors and Yields

According to a widely accepted scenario, classical novae are close binary systems consisting of a WD and a low mass MS star. The WD in the majority of the cases

is made of C and O (∼70%) and some are ONeMg WDs (∼30%). When the companion fills its Roche lobe, the WD accretes H-rich material and this triggers an explosive H-ignition. During the explosion, the rise in optical luminosity is as high as $(10^4$–$10^5)\, L_\odot$. Many hydrodynamical calculations of nova outbursts have shown that an important fraction of the accreted envelope is then ejected. Since the temperatures attained in the envelope during the explosion are rather high, approximately $(2 - 3) \times 10^8$ K, the ejecta show a significant nuclear processing. It has been shown that nova outbursts can be a site of ^{7}Li production, if the fast ^{7}Be transport mechanism operates. This mechanism was suggested by Cameron and Fowler (1971) and it works in this way: there must be a site where the $^3\mathrm{He}(\alpha, \gamma)^7\mathrm{Be}$ reaction, active during H-burning, can occur but ^{7}Be should be rapidly transported into regions where lower temperatures will allow it to decay into ^{7}Li by k-capture. During the explosive H-ignition CNO isotopes are also formed. But are novae really interesting objects relative to the study of Galactic chemical enrichment? The total mass ejected by classical novae over the Galaxy lifetime can be roughly estimated by considering the product of the observed Galactic nova rate (∼30 nova per year) by the the Galaxy lifetime (∼10 Gyr) and the average mass ejected per nova outburst $(\sim 2 \times 10^{-5} M_\odot)$. This gives $\sim 6 \times 10^6 M_\odot$ of total mass ejected by novae and it represents only a small fraction of the gas in the Galaxy. Therefore, from the point of view of the enrichment in global metals, the novae are negligible relative to other sources such as supernovae. However, for chemical elements such as ^{7}Li, ^{13}C, ^{15}N, and ^{17}O and radioactive isotopes such as ^{22}Na and ^{26}Al, novae can be important contributors. For example, novae can be the major producers of ^{15}N, as shown by several chemical evolution models, and could in principle contribute also to a nonnegligible fraction of ^{7}Li, although the ^{7}Li production in novae is quite uncertain and no clear observational evidence for ^{7}Li production by novae exists. From the chemical evolution point of view, the nova contribution becomes important only at late stages of the galactic evolution since the binary secondary star, which triggers the explosion when it fills its Roche lobe, is a low mass with a long lifetime.

2.1.4 Gas Flows

Gas flows in and out of galaxies are fundamental ingredients for studying their chemical evolution, since they are required to explain several important features in galaxies and galaxy clusters. These features include the metallicity distribution of G-dwarfs in the solar neighborhood, the abundance gradients along galactic disks as well as the heavy element abundances measured in the intracluster medium (ICM). We will discuss here the infall of gas onto disks, the radial flows along disks, and galactic winds.

2.1.4.1 Gas Infall

Oort in 1970 first discussed the possibility of matter infalling onto the disks of spiral galaxies. He envisioned that the penetration into the Galaxy of extragalactic neutral

gas clouds with very high velocities (VHVC; $|V| > 140\,\mathrm{km\,s^{-1}}$) can trigger the formation of high velocity clouds (HVC; $80 \leq |V|\,\mathrm{km\,s^{-1}} \leq 140$) when they interact with Galactic matter. He suggested that the present time infall rate onto the Galaxy should be of the order of $1 M_{\odot}\,\mathrm{yr}^{-1}$. Mirabel and Morras (1984, 1990) presented observations at 21 cm of HI in the direction of the galactic anticenter showing that a stream of VHVC has reached the outer Galaxy and is interacting with galactic matter. Their HI survey provided evidence for the accretion of gas onto the Galaxy at very high velocities: more than 99% of the VHVC in the direction of the galactic anticenter and 84% of the VHVC in the inner Galaxy have negative (approaching) velocities.

It should be noted that the computation of the infall rate onto the Galaxy depends on several unknown factors such as the distance to the clouds, the motion of the objects in the plane of the sky and the actual distribution of infalling gas over the whole sky and, therefore, the observational estimates of the infall rate should be regarded as still uncertain. Mirabel and Morras derived, from a survey of VHVC, a total infall rate onto the galactic disk of (0.2–0.5) $M_{\odot}\,\mathrm{yr}^{-1}$.

The origin of VHVC is not known but very probably they are made of extragalactic gas. On the other hand, HVC could have a Galactic origin, as originally proposed by Oort, and could have been set in motion by the interaction with the VHVC.

Analyses of intermediate, high, and very high velocity clouds (IVC, HVC, and VHVC) by means of UV, optical, and radio measurements along the line of sight of globular clusters and halo stars have shown that no cloud has a height z above the galactic plane lower than 300 pc. Therefore, this seems to rule out a local origin for all of these clouds, otherwise they should also be found at lower galactic latitudes and show $\sim$50% of positive velocities. It was also found that whilst the northern Galactic hemisphere shows many approaching clouds, the southern hemisphere is almost empty. This could be an indication of the intergalactic origin of the gas, captured only by the leading face of the Galaxy in its motion towards Virgo. The rate of gas infall extrapolated from these observations is around $(1-2) M_{\odot}\ \mathrm{yr}^{-1}$, obviously larger than that estimated from solely the VHVC.

In order to ascertain the origin of all these clouds it would be very important to measure their chemical composition (i.e., a roughly solar metallicity would prove a local origin), but the available data are not good enough to draw firm conclusions.

Braun and Burton (1999) have identified a particular class of HVC, which might represent a homogeneous subsample of these objects, in a single physical state. These clouds are compact (CHVC) and apparently isolated; they possess an infalling velocity of the order of $100\,\mathrm{km\,s^{-1}}$ in the Local Group reference frame. The interesting aspect of this study is that it suggests that the CHVC are probably not the consequence of a galactic fountain and that they rather have an extragalactic origin. They could represent examples of collapsed pristine gas with very little internal star formation and enrichment, the building blocks of galaxies in a hierarchical structure formation scenario.

In the past, the existence of infall onto the Galaxy has been challenged by the consideration that if the infalling gas stopped abruptly when hitting the disk, this energy should be radiated in the X-rays, at variance with the observed X-ray background. The temperature of the collisionally heated gas would be in the range of $(10^6$–$10^7)$ K for velocities in the range of 100–300 km s^{-1}, which would correspond to a radiation in the range $0.25 - -2.5$ keV. On the other hand, it has been argued that these soft X-ray photons would be absorbed by the interstellar HI after traveling a few parsecs through the Galactic disk, and that there is no chance of detecting the collisionally ionized gas. Finally, it has been suggested that HVCs and IVCs could be galactic fountains, namely, gas expelled out of the Galactic disk by SN explosions which later falls back onto the disk. Also in this case, to decide whether the gas comes from outside the Galaxy or it is a fountain one should look at the chemical abundances measured in such clouds.

From a theoretical point of view, the existence of infall of gas onto the Galactic disk was claimed as a natural consequence of a realistic galaxy formation process from extended halos, and to solve the G-dwarf problem in the solar vicinity. Infall is also desirable to prevent gas consumption in spirals in times shorter than their ages. Larson (1991) has shown that the infall rate of Mirabel and Morras, if transformed into a rate per unit area, by assuming (although it is very uncertain) that the infall rate is uniform over a disk of radius 15 kpc, gives $(0.3$–$0.7)M_\odot$ pc^{-2} Gyr^{-1}, which is only a fraction between 0.16 and 0.4 times the local gas depletion rate of $1.8M_\odot$ pc^{-2} Gyr^{-1}. The local gas depletion rate can be estimated by assuming that the average SFR in the last 12 Gyr has been $< \psi > \sim 3.5M_\odot$ pc^{-2} Gyr^{-1} and that the ratio $b = \psi(t_G)/ < \psi > \sim 0.5$. The past SFR is derived simply by subtracting from the solar neighborhood total surface mass density of $55M_\odot$ pc^{-2} the amount of gas of $13M_\odot$ pc^{-2} thus obtaining $42M_\odot$ pc^{-2}, which is roughly the mass turned into stars in the last 12 Gyr. Therefore, gas infall would increase the timescale for gas depletion between 16 and 40%. If these numbers are correct, the infall in the solar neighborhood should be a minor but not negligible effect at the present time. Finally, gas infall is important because of the significant presence of D in the solar neighborhood and in the Galactic center; in fact, D is only destroyed inside stars during galactic evolution and the present time D in the local ISM is instead very close to the primordial value, thus indicating that infall of primordial undepleted D must have occurred. The same conclusion can hold for the Galactic center where we expect practically no D at the present time, owing to the quite efficient SFR which should have taken place there, and instead we find a detectable amount of this element.

Unfortunately, the exact law for the gas accretion onto the Galaxy is not known and, in principle, it should be deduced from a good model of galaxy formation. The most simple scenario is to assume that the Galaxy formed by accretion of gas on a free-fall time, although we know that this is a too simplistic picture especially to explain the formation of the disk.

A more realistic representation of the infall rate is given by dynamical models for the formation of the Galaxy. Larson (1976), in his pioneering work, computed the formation of disk galaxies by means of hydrodynamical calculations including

rotation and axial symmetry. He found that the formation of spheroidal components requires shorter timescales than the formation of disks. The main parameters in his calculations are the collapse and the star formation rates, this latter being linked to the previous through the gas density. He pointed out that a fast star formation rate is required to form the spheroidal components whereas a much slower star formation rate is necessary in the disk to allow the gas to settle to a disk before forming stars. In particular, there should be a phase before the formation of the thin disk during which star formation was inhibited. However, this halt in the star formation still needs to be proven.

Moreover, Larson found that the timescale for the formation of the disk is much longer than the timescale for the formation of the spheroidal components (halo and bulge) and increases with increasing distance from the center; the inner parts of the disk form first, and the outer parts form progressively later as gas with higher and higher angular momentum settles into the equatorial plane at larger and larger radii (inside-out formation).

In models of galactic chemical evolution, we are forced to parametrize the infall rate because of the lack of a real dynamical treatment. Here we briefly summarize the most common parametrizations adopted in the literature for the infall rate (usually expressed in terms of surface gas density):

- Constant in space and time, which is obviously not very realistic
- Exponentially decreasing in time and constant in space
- Exponentially decreasing in time and also variable in space

In particular, Chiosi (1980) assumed an infall rate of primordial material of the form:

$$\left(\frac{\mathrm{d}\sigma_{\mathrm{gas}}}{\mathrm{d}t}\right)_{\mathrm{infall}} = a(r)\mathrm{e}^{-t/\tau}[M_{\odot}\ \mathrm{pc}^{-2}\ \mathrm{Gyr}^{-1}], \tag{2.30}$$

where τ is a parameter indicating the timescale for the accretion of the Galactic disk, and this parametrization was then adopted by many subsequent studies. The quantity τ is a free parameter since we do not have any specific indication about the mechanism of formation of the Galactic disk, and it can be assumed to be an increasing function of the galactocentric distance r, in order to account for the dynamical results of Larson. Matteucci and François (1989) adopted (2.30) for the infall law in the Galactic disk and suggested that the timescale of the infall τ is a linear function of the galactocentric distance, in the sense that it increases with the radius thus producing a situation of *inside-out* disk formation, as already suggested by Larson. The quantity $a(r)$ is obtained by imposing that (2.30) reproduces the present time observed exponential total surface mass density profile.

Generally, the chemical composition of the infalling material is assumed to be primordial, although there have been a few models adopting an enriched infall. It has been shown that the results obtained with enriched infall do not differ substantially from those obtained with primordial infall as long as the metallicity of the infalling gas does not exceed a critical value ($\sim 0.4\, Z_{\odot}$, Tosi (1988)). Enriched infall has often been claimed to explain the high astration

factor required for deuterium, if the observations suggesting a high primordial D abundance have to be trusted. In fact, an infall of gas enriched in heavy elements would be depleted in deuterium and a concentration of D lower than the primordial one in the accreting gas helps in diluting the abundance of D in the ISM. However, the most recent data do not favor high primordial D: in particular it is now widely adopted as a primordial D abundance of $D_p = (2.68^{+0.27}_{-0.25}) \cdot 10^{-5}$ (see Steigman (2007)).

- Other authors such as Lacey and Fall (1985) adopted an infall rate exponentially decreasing in time and radius:

$$A(r,t) = \frac{\alpha_f^2 M_{\rm D}(t_{\rm G})}{2\pi} \frac{{\rm e}^{(-\alpha_f r - t/\tau)}}{\tau[1 - {\rm e}^{(-t_{\rm G}/\tau)}]} [M_\odot \ {\rm yr}^{-1}], \tag{2.31}$$

where $M_{\rm D}(t_{\rm G})$ is the total mass of the disk at the present time $t_{\rm G}$ and α_f and τ are two adjustable parameters. The exponential radial dependence is chosen in order to obtain an exponential surface density profile at the present time.

- Chiappini et al. (1997) introduced the concept of double infall to explain the evolution of the halo thick-disk on one side and that of the thin disk on the other. In particular, they assumed that the halo thick-disk formed first by means of a relatively fast infall episode whereas the thin disk formed by means of a completely independent subsequent infall episode occurring on much longer timescales. In this way, the Galactic disk is almost completely formed out of extragalactic primordial gas (see also Chap. 5).

  The functional form of the infall rate they proposed is:

$$\left(\frac{{\rm d}\sigma_{\rm gas}}{{\rm d}t}\right)_{\rm halo\,thick\text{-}disk} \propto {\rm e}^{-t/\tau_1} \tag{2.32}$$

$$\left(\frac{{\rm d}\sigma_{\rm gas}}{{\rm d}t}\right)_{\rm thin\text{-}disk} \propto {\rm e}^{-(t - t_{\rm max})/\tau_2}, \tag{2.33}$$

where τ_1 and τ_2 are the timescale for the formation of halo thick-disk and thin disk, respectively, and $t_{\rm max}$ represents the time of maximum gas accretion onto the Galactic disk.

- The infall laws described before are clearly approximations with parameters that should be tuned to reproduce the present time infall rate in galaxies. In principle, the gas infall law should depend on the dark matter halo of each galaxy. Following this idea, cosmological N-body simulations have been performed in the ΛCDM scenario with the goal of finding the history of the assembly of a dark matter halo which could be the one of the Milky Way. Once found the possible halos for the Milky Way, the assumption is that the cold gas, falling into the potential well of the dark matter halo to form the Galactic disk, must have followed the same accretion law found for the dark matter halo.

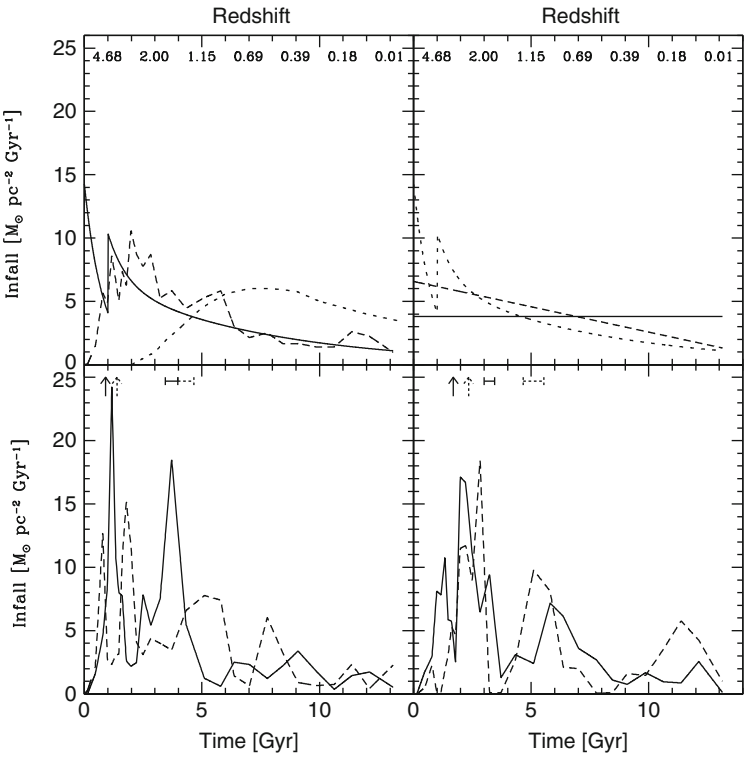

Fig. 2.15 Various infall laws for the Milky Way. The dark matter halos were selected by assuming a mass between 5×10^{11} and $5 \times 10^{12} M_{\odot}$. In the *top left panel* is shown the two-infall law for gas accretion (*continuous line*): the first infall episode is responsible for the formation of the halo thick-disk, whereas the second infall episode is responsible for the formation of the thin disk (Chiappini et al. 1997). Here, $\tau_1 = 2$ Gyr and $\tau_2 = 8$ Gyr. In the *lower left panel* is shown the best accretion cosmological law (*continuous line*) as derived by Colavitti et al. (2008). As one can see, the two laws are remarkably quite similar. The *dotted line* in the *upper left* panel is the infall law suggested by Naab and Ostriker (2006, their model 10). The *continuous line* in the *upper right panel* represents a constant infall rate, whereas the *dashed line* is a linear infall law and the dotted line is again the two infall law. The *dashed* and continuous lines in the *lower panels* are other cosmological laws derived by Colavitti et al. The assumed cosmology is ΛCDM. Figure from Colavitti et al. (2008)

This cosmologically derived infall law can be written as:

$$\frac{\mathrm{d}\sigma_{\mathrm{gas}}}{\mathrm{d}t} = a(r)0.19\frac{\mathrm{d}M_{\mathrm{DM}}}{\mathrm{d}t}[M_{\odot}\ \mathrm{pc}^{-2}\ \mathrm{Gyr}^{-1}] \tag{2.34}$$

with 0.19 being the cosmological baryonic fraction (the baryonic mass of the Galaxy being $M_{\mathrm{Gal}} = 0.19 M_{\mathrm{DM}}$) and M_{DM} the mass of the dark matter halo. In Fig. 2.15, we show cosmological and parametric infall laws compared to the two-infall law of (2.32) and (2.33). Among the cosmological infall laws, the one shown in the lower left panel of Fig. 2.15 is considered the best to reproduce the

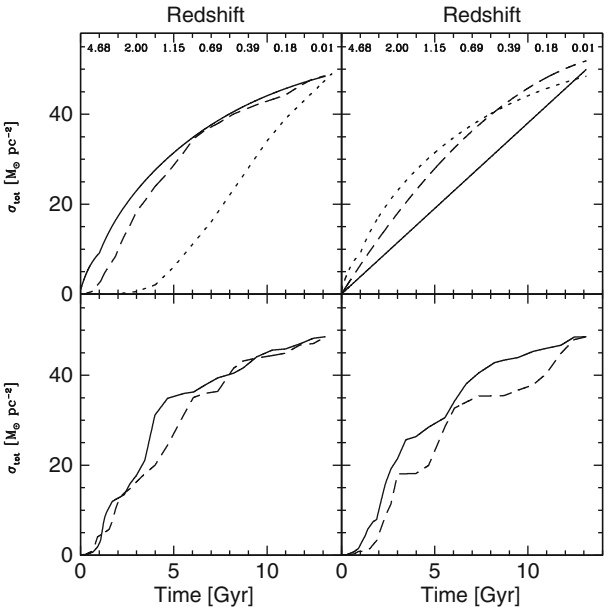

Fig. 2.16 Baryonic mass accumulation vs. time and redshift for the infall laws of Fig. 2.15. The *line symbols* are the same as for Fig. 2.15. The assumed cosmology is ΛCDM. Figure from Colavitti et al. (2008)

dark matter halo of the Milky Way and is very similar to the two-infall law, shown in the upper right panel. As one can see, in both infall laws there are two main peaks corresponding to the maximum accretion giving rise to the halo thick-disk first and the thin disk later.

In Fig. 2.15 are also shown simple parametric infall laws such as a constant infall rate and a linear infall law: none of those laws can reproduce at best the chemical properties of the Milky Way. In Fig. 2.16, we report the growth of the total surface mass density with time according to the laws in Fig. 2.15.

2.1.4.2 Radial Gas Flows

From the physical point of view, radial flows along galactic disks should be expected on the basis of the following arguments:

- The gas infalling onto the disk can induce radial inflows by transferring angular momentum to the gas in the disk, if its angular momentum is lower than that of the gas in the disk. Mayor and Vigroux (1981) showed that in this situation a radial inward gas motion, with velocity of the order of 1 to 5 km s^{-1}, is created for an infall rate of the order of $1 M_\odot$ yr^{-1} over the whole Galaxy.

- Angular momentum transfer due to the gas viscosity in the disk may induce inflows in the inner parts of the disk and outflows in the outer parts. This case was studied by Clarke (1989), who considered no external infall of gas and studied the evolution of the gas distribution in the Galactic disk in the presence of gas viscosity and a threshold in the star formation in the outer parts of the disk.
- Gravitational interactions between the disk gas and the spiral density waves can lead to large-scale shocks, dissipation, and radial flows with typical velocities of $\sim 3\,\mathrm{km\,s^{-1}}$.

Many authors have studied the effects of radial flows on the chemical evolution of galactic disks, in particular on the development of abundance gradients and gas distribution. Generally, they all agreed in concluding that radial inflows can help in building up abundance gradients under specific conditions concerning the velocity of the gas flow. However, other causes for abundance gradients must exist. Lacey and Fall concluded that radial inflows with velocities not larger than $2\,\mathrm{km\,s^{-1}}$ contribute to the creation of negative abundance gradients but only if the dependence of the star formation rate on the gas density is linear. Clarke concluded that, in the absence of external infall, low velocity radial flows induced by gas viscosity and coupled with a threshold in the star formation at large galactocentric distances (18 kpc) can well-reproduce the abundance gradient and the gas distribution along the Galactic disk. Edmunds and Greenhow (1995) showed that there is no simple "one-way" effect of flows on gradients, although in the linear star formation case accelerating inflows tend to flatten the gradients while decelerating inflows tend to steepen them.

Observations of gas along the Galactic disk seem to be consistent with radial flows of modest velocities up to few $\mathrm{km\,s^{-1}}$; the local HI appears to be at rest relative to the local standard of rest (LSR) to within about $1\,\mathrm{km\,s^{-1}}$ (Kerr 1969; Crovisier 1978). Concerning the molecular clouds within a few kpc of the Sun, a mean inward motion of roughly $4\,\mathrm{km\,s^{-1}}$ is found (Stark 1984).

2.1.4.3 Gas Outflow

Gas outflows are likely to play a fundamental role in the evolution of galaxies, and their existence is indicated by several observational constraints. Galactic outflows are now observed in dwarf irregular starburst galaxies and the chemical composition of the ICM (measured from X-ray emission lines) shows an almost solar iron abundance indicating that the galaxies in clusters should loose a substantial amount of their ISM. Galactic outflow can eventually leave the potential well of galaxies and then they are called *galactic winds*. Otherwise, the gas outflowing can remain bound to the galaxies and even fall back into the disk; in such a case, we have the so-called *galactic fountains*.

The main cause for galactic winds are the supernovae which can trigger gas outflows when the thermal content of the gas, resulting from energy deposition from their explosions, equals its binding energy. This is a necessary condition for the

occurrence of the wind but not sufficient, in fact, for a wind to really develop, the energy deposited into the ISM should not be radiated away. To this purpose, a good condition is that all the supernova remnants should overlap, in other words that the filling factor should be equal to unity. In this situation, in fact, the SNe of the second generation would explode in a rarified and hot medium and transfer the maximum energy since the radiation is proportional to the square of the gas density. Stellar winds from massive stars also contribute to the heating of the ISM, although their contribution, in most of the astrophysical situations, is substantially smaller than that of supernovae, with the exception of the very early stages of a starburst where they can dominate the energetics.

Supernova-driven galactic wind models have become very popular in the last years since they seem to reproduce well the chemical and photometric properties of elliptical galaxies, together with the observed abundances of heavy elements in the ICM and the observed scatter in the properties of dwarf irregular and blue compact galaxies. The ordinary galactic wind is made of ambient ISM, where the metals produced and ejected by stars are normally well-mixed with the pre-existing medium. Therefore, in general, the element abundances in the wind should reflect those of the ISM. However, supernova explosions can produce chimneys which eject outside the galaxy mostly the SN ejecta, namely, metal enriched material. This process can give rise to the so-called *metal-enhanced or biased winds*. This is very likely to occur in dwarf starburst galaxies because of their lower potential well.

However, it is very difficult to assess how much energy is deposited from winds and supernovae into the ISM and how much is lost (these processes are generically called *feedback*). This is a key problem in galaxy formation and evolution that will certainly be developed in the future thanks to the advent of more and more sophisticated dynamical and chemical evolution models. Another fundamental parameter which enters in the development of a galactic wind is the potential well of the considered galaxy and, therefore, involves the problem of dark matter halos.

In galactic chemical evolution models, we can only parametrize the galactic winds and here we recall the most common parametrizations :

- A continuous wind rate proportional to the SFR, a formulation which has been applied in models predicting the evolution of starburst galaxies, namely:

$$\left(\frac{\mathrm{d}\sigma_{\mathrm{gas}}}{\mathrm{d}t}\right)_{\mathrm{wind}} = \lambda\psi(t), \tag{2.35}$$

  where w is a free parameter measuring the *efficiency* of the galactic wind. If we want to express the rate of galactic wind per chemical element, i, we can write:

$$\left(\frac{\mathrm{d}\sigma_{\mathrm{gas}}X_i}{\mathrm{d}t}\right)_{\mathrm{wind}} = \lambda_i\psi(t), \tag{2.36}$$

  where X_i is the ISM abundance of the element i. The efficiency λ_i is assumed to be constant in a normal wind, while different efficiencies for different elements characterize a metal-enhanced wind (see next chapters). In other words, one

can assume that mostly metals are lost in a galactic wind. Enriched galactic winds can explain some anomalous abundance ratios observed in some starburst galaxies, such as for example the dwarf galaxy IZw18, where it is observed an almost solar N/O ratio, very difficult to reproduce by adopting the standard stellar nucleosynthesis and normal galactic winds. Another example is the high $\Delta Y/\Delta Z$ ratio (namely, the enrichment of helium relative to metals during the galactic lifetime) observed in dwarf irregular and blue compact galaxies. In this case, an enriched wind, of the type described before, produces a good agreement with the observed $\Delta Y/\Delta Z$.

- A sudden wind occurring when the thermal energy of the gas exceeds its binding energy and all the gas present is lost. This is the case of the supernova-driven models adopted by some authors for studying the evolution of elliptical galaxies.

Observationally, galactic winds have been detected in dwarf irregular galaxies by comparing the speed of the observed gas outflow with the galaxy escape velocity and the suggestion is that the gas outflows at a rate proportional to the SFR (see Chap. 7).

http://www.springer.com/978-3-642-22490-4

Chemical Evolution of Galaxies
Matteucci, F.
2012, XIV, 226 p., Hardcover
ISBN: 978-3-642-22490-4